PHYSICAL REVIEW B VOLUME 13, NUMBER 6 15 MARCH 1976

Compton profiles of LiF

K.-F. Berggren
Department of Physics, Linköping University, S-581 83 Linköping, Sweden

F. Martino
Department of Physics, The City College of the City University of New York, New York, New York 10031

P. Eisenberger and W. A. Reed
Bell Laboratories, Murray Hill, New Jersey 07974
(Received 30 September 1975)

γ-ray Compton profiles of LiF with the scattering vector along the $\langle 100\rangle$, $\langle 110\rangle$, and $\langle 111\rangle$ axes are reported. Both the absolute profiles and their anisotropy are derived from a tight-binding model and compared with experiments. The overall agreement between theory and experiment is found to be satisfactory for all three directions. Recent calculations of Euwema *et al.* are compared with the present work and found to predict incorrect anisotropies, particularly at small momentum transfers. It is also shown that momentum distributions can be orders of magnitude more sensitive to anisotropy in the electron distributions than x-ray structure factors, at least in materials where overlap of the wave functions is small.

I. INTRODUCTION

In previous papers we have reported Compton profiles and anisotropic momentum distributions in covalent bonded solids.[1,2] In these crystals relatively large anisotropies exist. This naturally raises the question as to the degree of anisotropy which exists in highly ionic crystals. Although Compton profiles have been reported on a number of ionic crystals only Weiss[3] has previously looked for anisotropy. His conclusion for LiF was that to within 2% there was no significant anisotropy. Owing to the greater precision attainable using γ rays we decided to remeasure LiF and try to place smaller error limits on the measurements.

There are also other reasons for studying LiF. The ground state may simply be viewed as a superposition of closed-shell ions which overlap each other only very weakly. For theory LiF is therefore one of the simplest systems available since an extreme tight-binding (or Heitler-London) model is likely to yield a highly accurate description of its electronic structure. Besides that the number of electrons per ion is small. For some time now a series of calculations of total energy, lattice constants,[4,5] form factors,[6] isotropic Compton profiles,[7-9] etc., have indeed achieved substantial agreement with experiments with such a description. This indicates, furthermore, that electronic correlation may be less important in describing ground-state properties. We are therefore dealing with a rather ideal case; the total wave function is simple and accurate, and hence the anisotropic Compton profile can be computed with high precision and with relative ease. Thus LiF should offer a beautiful opportunity for studying the various assumptions which are incorporated in the Compton-scattering technique, such as the impulse approximation, relativistic, and multiple-scattering corrections. Still another reason for the present study is a recent Hartree-Fock calculation of the directional Compton profiles by Euwema *et al.*[10] A brief report by the present authors may be found in Ref. 11.

Section II describes the experiment and some basic assumptions made in the Compton-scattering technique. The experimental results are given in Sec. III. A tight-binding model is discussed in Sec. IV and the derivation of the directional Compton profile for this particular model is outlined. Using a basis consisting of Slater-type orbitals it is found that the calculations can be performed analytically. Numerical results are presented in Sec. V. A discussion is given in Sec. VI and a summary in Sec. VII. Appendices A and B contain mathematical details.

II. EXPERIMENT

A. Compton-scattering theory

The theory of the Compton-scattering cross section and the validity of the impulse approximation have been previously described[12-14] so that we will only list the important relations. From Ref. 14 we have

$$\frac{d\sigma}{d\Omega\, d\omega_2} = \frac{r_0^2 mc\,\omega_2 \bar{X} J(q)}{2\omega_1[(\omega_1^2+\omega_2^2-2\omega_1\omega_2\cos\theta)^{1/2}+(q/mc)(\omega_1-\omega_2)]}, \tag{1}$$

where

$$\bar{X} = \frac{\omega_1(1+q/mc)}{\omega_2(1-q/mc)} + \frac{\omega_2(1-q/mc)}{\omega_1(1+q/mc)}, \tag{2}$$

$$q = \frac{(\vec{k}_1 - \vec{k}_2) \cdot \vec{p}_0}{|\vec{k}_1 - \vec{k}_2|} = 137 \frac{\omega_1 - \omega_2 - \omega_1\omega_2(1-\cos\theta)/mc^2}{(\omega_1^2 + \omega_2^2 - 2\omega_1\omega_2\cos\theta)^{1/2}} \; , \tag{3}$$

$$J(q) = \int n(\vec{p})\, dp_\alpha\, dp_\beta \; , \tag{4}$$

and

$$\vec{p}_\alpha \cdot \vec{k} = \vec{p}_\beta \cdot \vec{k} = \vec{p}_\alpha \cdot \vec{p}_\beta = 0 \; . \tag{5}$$

Here we denote the energy and momentum of the incident and scattered photon by ω_1, $\vec{k}_1$ and ω_2, $\vec{k}_2$, respectively, and $\hbar = 1$. Our total profiles (including core) are normalized such that

$$\int_0^{15} J(q)\, dq = 6 \text{ electrons} \tag{6}$$

for LiF. (In Sec. IV we shall use the notation p_z for q.)

B. Experimental details

The basic experiment consists of scattering 159-keV γ rays from the sample, detecting the radiation scattered at 173° with a Ge(Li) detector, and recoding the signal on a multichannel analyzer. A description of the apparatus and data processing is contained in Refs. 1, 15, and 16.

To measure the absolute profile we used 2.54-cm square, single-crystal plates 0.178- and 0.307-cm thick. The ⟨100⟩ crystallographic axis was normal to the plane of the plates. Approximately 50 000 and 100 000 counts were collected in the peak for the two samples, respectively. To better compare our experimental results with theoretical calculations we report our absolute profile data both with and without correction for the finite resolution of our spectrometer.

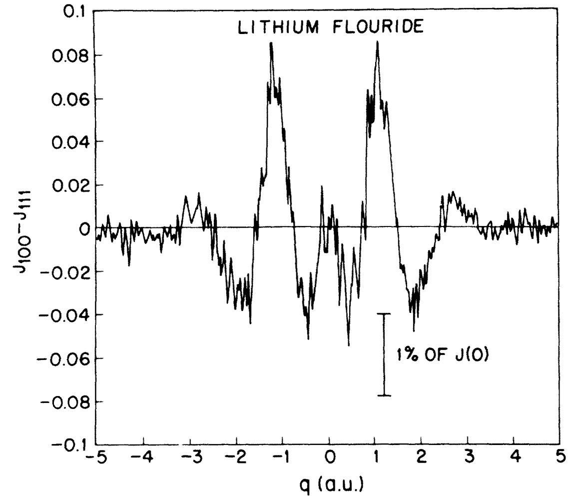

FIG. 1. Point-by-point subtraction of ⟨100⟩ and ⟨111⟩ measurements after normalization and background subtraction.

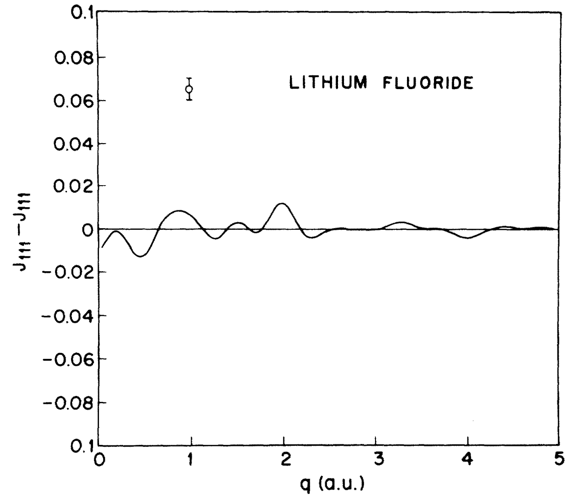

FIG. 2. Difference between two independent ⟨111⟩ measurements processed in the same manner as the results in Fig. 3–5.

The anisotropy measurements were made on a 1.27-cm diam single-crystal cylinder, 2.54 cm in length with the ⟨110⟩ axis parallel to the cylinder axis. Measurements were made with the scattering vector parallel to the ⟨100⟩, ⟨110⟩, and ⟨111⟩ axes and in each case approximately 180 000 counts were collected in the peak. For each direction two measurements were made, the data processed separately to ensure they were the same (to within our experimental error), and then averaged. The anisotropy data were processed in the manner described in Ref. 16. The profiles were first subtracted, averaged over $\pm q$, and then smoothed with a digital filter. The anisotropy data were not corrected for the resolution of the spectrometer since we feel that is better to convolve the theory with our resolution function than try to remove the effect of resolution from the data. Our resolution function is

$$R(q) = (1/\sigma\sqrt{2\pi})\, e^{-(1/2)[(q-q_0)/\sigma]^2} \; , \tag{7}$$

where $\sigma = 0.202$ a.u.

In Fig. 1 we show the difference between J_{100} and J_{111} before smoothing. The anisotropy is readily apparent and is symmetric for positive and negative values of q. The difference is essentially zero for large values of $|q|$ which also indicates that no spurious effects are present. After averaging and smoothing the data we estimate the mean-square deviation of the difference data to be ± 0.006 (see Fig. 2).

III. EXPERIMENTAL RESULTS

In Table I we present the absolute profiles for LiF for the scattering vector parallel to ⟨100⟩ for our 0.178-cm thick sample with and without resolu-

TABLE I. Experimental Compton profiles for LiF—⟨100⟩.

q (a.u.)	Thickness (cm) 0.178[a]	0.178[b]	0.0[a]	0.0[b]
0	3.776 ± 0.035	3.711 ± 0.035	3.876	3.807
0.1	3.764	3.699	3.861	3.791
0.2	3.713	3.652	3.805	3.737
0.3	3.626	3.570	3.710	3.648
0.4	3.509	3.459	3.587	3.532
0.5	3.372	3.372	3.443	3.393
0.6	3.219	3.179	3.281	3.239
0.7	3.048	3.014	3.103	3.068
0.8	2.857	2.830	2.900	2.875
0.9	2.645	2.627	2.678	2.663
1.0	2.418 ± 0.024	2.412 ± 0.024	2.438	2.438
1.1	2.188	2.194	2.196	2.209
1.2	1.962	1.980	1.958	1.985
1.3	1.748	1.776	1.734	1.773
1.4	1.551	1.586	1.530	1.578
1.5	1.374	1.412	1.350	1.398
1.6	1.219	1.258	1.196	1.240
1.7	1.086	1.123	1.064	1.101
1.8	0.973	1.007	0.951	0.982
1.9	0.879	0.908	0.858	0.882
2.0	0.800 ± 0.008	0.825 ± 0.008	0.780	0.798
2.2	0.667	0.692	0.648	0.663
2.5	0.541	0.547	0.524	0.517
3.0	0.366	0.371	0.351	0.344
3.5	0.255	0.259	0.243	0.237
4.0	0.197	0.198	0.188	0.183
5.0	0.119 ± 0.003	0.120 ± 0.002	0.115	0.117
6.0	0.077	0.077	0.075	0.076
7.0	0.051	0.051	0.050	0.051
8.0	0.034	0.034	0.034	0.034
9.0	0.022	0.022	0.022	0.022
10.0	0.017 ± 0.002	0.017 ± 0.002	0.017	0.017
15.0	0.004	0.064	0.004	0.004
20.0	0.001	0.001	0.001	0.001
25.0	0.000	0.000	0.000	0.000

[a] Corrected for spectrometer resolution.
[b] No resolution correction.

tion correction and the same profiles after removing our estimate of the effects of multiple scattering. Our estimate of multiple scattering was obtained by measuring a 0.307-cm sample as well as the 0.178-cm thick one and extrapolating their difference to zero thickness.[17] As can be seen the multiple-scattering correction is about 2.5% at $q = 0$.

In Table II we list the anisotropy measured for $J_{100} - J_{110}$, $J_{100} - J_{111}$, and $J_{110} - J_{111}$ and in Figs. 3–5 these results are illustrated as solid lines. The data in both the table and the figures have been corrected for multiple scattering but the resolution broadening of the spectrometer has not been removed. The effect of multiple scattering is, to first order, only to decrease the amplitude of the measured anisotropy and not alter its shape since any photon scattered more than once is expected to lose its orientational information.[1] The percentage of photons multiply scattered can be estimated from both a simple calculation which ignores photoelectric losses and an analysis of data taken on samples as a function of thickness. The calculation gives an amplitude enhancement factor for the anisotropy of 1.27 whereas the analysis of the experimental data gives a factor of 1.28. Since our experimental accuracy for the anisotropy is ±12% of the peak-to-peak anisotropy a 1% uncertainty in the multiple-scattering correction is well within our stated error.

IV. THEORETICAL EVALUATION OF THE COMPTON PROFILE

A. Tight-binding model

In a crystal like LiF the overlap between the charge distributions centered at the different ions

TABLE II. Anisotropy of LiF Compton profiles with no resolution correction.

q (a.u.)	$J_{100} - J_{110}$	$J_{100} - J_{111}$	$J_{110} - J_{111}$
0	0.028	0.002	−0.026
0.1	0.018	−0.002	−0.020
0.2	0.003	−0.012	−0.015
0.3	−0.011	−0.024	−0.013
0.4	−0.019	−0.032	−0.013
0.5	−0.022	−0.035	−0.012
0.6	−0.019	−0.029	−0.009
0.7	−0.011	−0.015	−0.004
0.8	0.002	0.008	0.006
0.9	0.018	0.036	0.018
1.0	0.030	0.059	0.029
1.1	0.036	0.070	0.034
1.2	0.038	0.067	0.029
1.3	0.037	0.053	0.017
1.4	0.030	0.031	0.001
1.5	0.018	0.007	−0.011
1.6	0.003	−0.015	−0.018
1.7	−0.011	−0.030	−0.020
1.8	−0.021	−0.037	−0.016
1.9	−0.028	−0.038	−0.009
2.0	−0.033	−0.033	−0.000
2.1	−0.035	−0.025	0.010
2.2	−0.033	−0.018	0.015
2.3	−0.026	−0.012	0.014
2.4	−0.015	−0.005	0.010
2.5	−0.003	0.002	0.005
2.6	0.008	0.008	0.000
2.7	0.015	0.011	−0.004
2.8	0.017	0.012	−0.005
2.9	0.014	0.009	−0.005
3.0	0.010	0.006	−0.003
3.1	0.006	0.004	−0.002
3.2	0.002	0.002	0.000
3.3	−0.003	0.000	0.002
3.4	−0.006	−0.002	0.004
3.5	−0.007	−0.003	0.003
3.6	−0.005	−0.004	0.001
3.7	−0.002	−0.003	−0.001

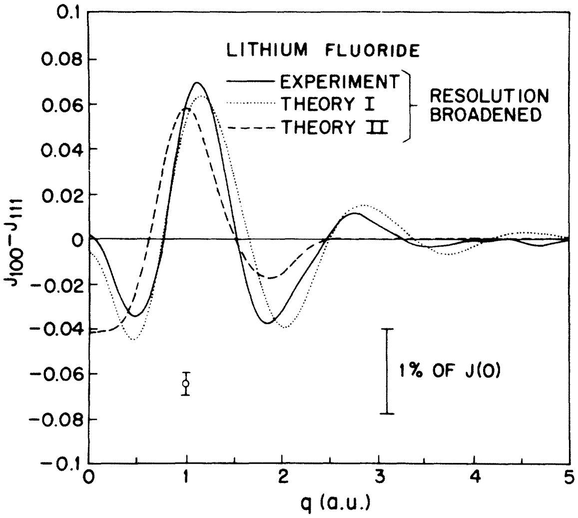

FIG. 3. Smoothed and ±*q* averaged difference of the data for ⟨100⟩ and ⟨111⟩ directions shown in Fig. 1. Theory of Euwema *et al.* smeared with our resolution function is shown as a dashed line (II). The present theory using Kunz's crystal orbitals and smeared in the same way is shown as a dotted line (I).

is small. It is therefore a good first approximation to let the total crystal wave function be the single determinant

$$\Phi(\vec{r}_1, \vec{r}_2, \ldots, \vec{r}_N) = (1/\sqrt{N!})\det[\chi_\alpha^g(\vec{r})]\,, \tag{8}$$

where

$$\chi_\alpha^g(\vec{r}) = \chi_\alpha(\vec{r} - \vec{R}_g) \tag{9}$$

are undistorted free ion solutions centered at the different lattice sites $\vec{R}_g$. Index α denotes the quantum numbers (nlm). The first-order density matrix is then[5]

$$\hat{\rho} = 2\sum_\alpha^g \sum_\beta^h |\chi_\alpha^g\rangle (\tilde{\Delta}^{-1})^{g,h}_{\alpha,\beta} \langle \chi_\beta^h| \ . \tag{10}$$

Here the g and h summations refer to all occupied states α and β at sites $\vec{R}_g$ and $\vec{R}_h$, respectively. The factor of 2 comes from spin and $\tilde{\Delta}^{-1}$ is the inverse of the overlap matrix. Since the off-diagonal elements in $\tilde{\Delta}$ are small, the expansion[5]

$$\tilde{\Delta}^{-1} = (1 + \tilde{S})^{-1} = 1 - \tilde{S} + \tilde{S}^2 \mp \cdots \tag{11}$$

is usually made. To second order in S we then have the properly normalized density matrix

$$\hat{\rho} = 2\sum_\alpha^g |g, \alpha\rangle\langle g, \alpha| - 2\sum_\alpha^g \sum_\beta^h |g, \alpha\rangle S^{g,h}_{\alpha,\beta} \langle h, \beta| + 2\sum_{\alpha,\beta}^g |g, \alpha\rangle (\tilde{S}^2)^{g,g}_{\alpha,\beta} \langle g, \beta| \ , \tag{12}$$

where

$$S^{g,h}_{\alpha,\beta} = \langle g, \alpha | h, \beta\rangle - \delta_{g,h}\,\delta_{\alpha,\beta} \tag{13}$$

and $|g, \alpha\rangle$ corresponds to the orbital $\chi_\alpha(\vec{r} - \vec{R}_g)$. Throughout this work we have used real orbitals.

In a refined version of the tight-binding model the free ion solutions are allowed to relax in accordance with the crystal environment. By means of the Adams-Gilbert[18,19] local orbital scheme and an expansion like Eq. (12), Kunz[20] has computed such self-consistent orbitals for LiF. We shall investigate both types of orbitals.

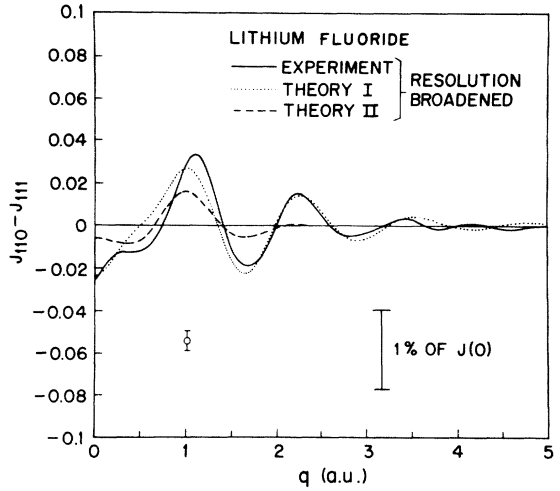

FIG. 5. Difference between ⟨110⟩ and ⟨111⟩ Compton profiles after smoothing and averaging ±*q* results (solid line). Theory of Euwema *et al.* smeared with our resolution function is shown as a dashed line (II). The present theory using Kunz's crystal orbitals and smeared in the same way is shown as a dotted line (I).

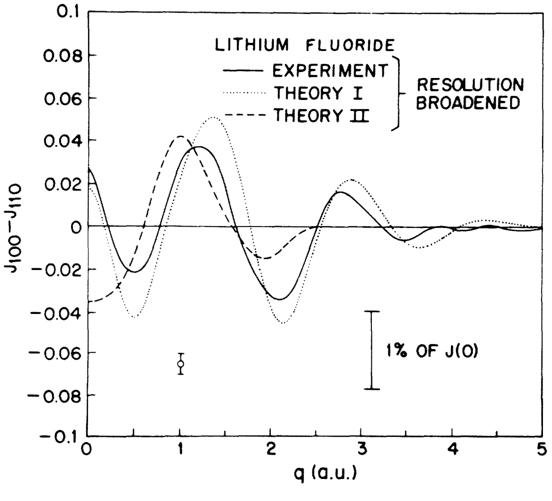

FIG. 4. Difference between ⟨100⟩ and ⟨110⟩ Compton profiles after smoothing and averaging ±*q* results (solid line). The theory of Euwema *et al.* smeared with our resolution functions is shown as a dashed line (II). The present theory using Kunz's crystal orbitals and smeared in the same way is shown as a dotted line (I).

B. Momentum density and Compton profile

The momentum density of the system is in general defined as

$$n(\vec{p}) = \langle \vec{p} \,|\, \hat{\rho} \,|\, \vec{p} \rangle \ , \tag{14}$$

where $|\vec{p}\rangle$ stands for a plane-wave state normalized as $\langle \vec{p} \,|\, \vec{p}\,' \rangle = \delta(\vec{p} - \vec{p}\,')$. The momentum density of an ion, a F$^-$ ion for example, is then from Eqs. (12) and (14)

$$n_{\mathrm{F}^-}(\vec{p}) = 2 \sum_{\alpha}^{0} \sum_{\beta}^{0} [\delta_{\alpha\beta} + (\tilde{S}^2)^{0,0}_{\alpha,\beta}] \langle \vec{p} \,|\, \alpha \rangle \langle \beta \,|\, \vec{p} \rangle - 2 \sum_{\alpha}^{0} \sum_{\beta}^{h} \langle \vec{p} \,|\, \alpha \rangle S^{0,h}_{\alpha,\beta} \langle \beta \,|\, \vec{p} \rangle e^{-i\vec{p}\cdot\vec{\mathrm{R}}_h} \ , \tag{15}$$

where

$$\langle \vec{p} \,|\, \alpha \rangle = \frac{1}{(2\pi)^{3/2}} \int d\vec{r}\, e^{i\vec{p}\cdot\vec{r}} \chi^0_\alpha(\vec{r}) \tag{16}$$

defines the momentum transform of an orbital at the central site 0. There is no restriction in chosing the ion as the central one as in Eq. (15).

Using Eq. (15), it is then convenient to write the Compton profile [Eq. (4)] (with $p_z \equiv q$)

$$J_{\mathrm{F}^-}(p_z) = J^0_{\mathrm{F}^-}(p_z) + J^1_{\mathrm{F}^-}(p_z) + J^2_{\mathrm{F}^-}(p_z) \ , \tag{17}$$

where

$$J^0_{\mathrm{F}^-}(p_z) = 2 \int \int dp_x \, dp_y \sum_{\alpha}^{0} |\langle \vec{p} \,|\, \alpha \rangle|^2 \ , \tag{18}$$

$$J^1_{\mathrm{F}^-}(p_z) = -2 \int \int dp_x \, dp_y \sum_{\alpha}^{0} \sum_{\beta}^{h} \langle \vec{p} \,|\, \alpha \rangle \times S^{0,h}_{\alpha,\beta} \langle \beta \,|\, \vec{p} \rangle e^{-i\vec{p}\cdot\vec{\mathrm{R}}_h} \ , \tag{19}$$

$$J^2_{\mathrm{F}^-}(p_z) = 2 \int\int dp_x \, dp_y \sum_{\alpha,\beta}^{0} (\tilde{S}^2)^{0,0}_{\alpha,\beta} \langle \vec{p} \,|\, \alpha \rangle \langle \beta \,|\, \vec{p} \rangle . \tag{20}$$

Similar expressions hold for the Li$^+$ ion, so that the total profile is

$$J(p_z) = J_{\mathrm{Li}^+}(p_z) + J_{\mathrm{F}^-}(p_z) \ . \tag{21}$$

In the elementary version of the tight-binding model J^0 clearly represents a superposition of free ions, whereas J^1 and J^2 represent the solid-state effects. Therefore J^0 is independent of the direction of the scattering vector, so we may write

$$J^0(p_z) = 2\pi \int_{|p_z|}^{\infty} dp \, p \sum_{\alpha}^{0} |\langle \vec{p} \,|\, \alpha \rangle|^2 \ . \tag{22}$$

Equation (22) is also true for Kunz's orbitals.^{20}

We shall now consider the evaluation of J^1 and J^2 separately.

C. Evaluation of $J^1(p_z)$

To display the angular dependence of the transforms $\langle \vec{p} \,|\, \alpha \rangle$ explicitly we use the notations

$$\langle \vec{p} \,|\, s \rangle = \chi_s(p) \tag{23}$$

for the s orbitals, and

$$\langle \vec{p} \,|\, 2p \rangle = i\chi_{2p}(p)\,\vec{p} \tag{24}$$

for the $2p$ orbitals [for Eqs. (23) and (24) see Appendix A, Eqs. (A4) and (A6)].

To begin with we may take the $2p$ orbitals at all the lattice sites to be oriented in the same way in configuration space, namely, along the three axes of a Cartesian coordinate system (I) with its z axis along the scattering vector $\vec{\mathrm{S}}$ (see Fig. 6). Equation (24) indicates that the $2p$ orbitals are oriented in the same way in momentum space. In order to evaluate the integral in Eq. (19) over the xy plane it is convenient, however, to introduce another coordinate system (II) which is different for each pair of ions. For this purpose let the lattice vector $\vec{\mathrm{R}}_h$ be written

$$\vec{\mathrm{R}}_h = \vec{\mathrm{R}}_{h,\perp} + \vec{\mathrm{R}}_{h,\parallel} \ , \tag{25}$$

where $\vec{\mathrm{R}}_{h,\perp}$ is the component along the z axis and $\vec{\mathrm{R}}_{h,\parallel}$ the component in the xy plane. The new coordinate system is then obtained by the rotation around the z axis which brings the x axis along $\vec{\mathrm{R}}_{h,\parallel}$ (see Fig. 6). In Appendix B it is shown that the sum

$$\sum_{\alpha}^{0} \sum_{\beta}^{h} \langle \vec{p} \,|\, \alpha \rangle S^{0,h}_{\alpha,\beta} \langle \beta \,|\, \vec{p} \rangle \tag{26}$$

is invariant under such a transformation. Introducing cylindrical coordinates we may now write (see Fig. 6)

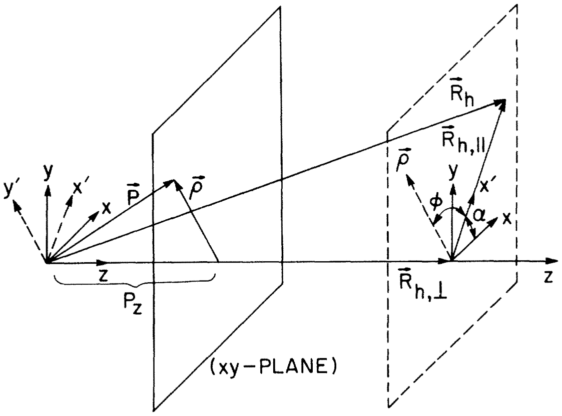

FIG. 6. Plane of integration is the xy plane at p_z, and is perpendicular to the scattering vector $\vec{\mathrm{S}}$ oriented along the z axis. The vector $\vec{\mathrm{R}}_h = \vec{\mathrm{R}}_{h,\perp} + \vec{\mathrm{R}}_{h,\parallel}$, with $\vec{\mathrm{R}}_{h,\perp}$ and $\vec{\mathrm{R}}_{h,\parallel}$ perpendicular to and parallel with the xy plane, respectively, denotes a lattice site. In order to perform the integration it is convenient to make a coordinate transformation from the (xyz) system (I) to the $(z'y'z')$ system (II), which is such that $\vec{\mathrm{R}}_{h,\parallel}$ and the x' axis coincide. System (I) is defined by the direction of the scattering vector and is the same for all sites $\vec{\mathrm{R}}_h$, whereas system (II) is different for each pair of ions.

$$\vec{\mathrm{p}}\cdot\vec{\mathrm{R}}_h=\rho R_{h,\parallel}\cos(\phi)+p_z R_{h,\perp}\quad . \tag{27}$$

The integration over the angular parts can now easily be performed, resulting in cylindrical Bessel functions $J_l(\rho R_{h,\parallel})$. For example, for the first shell and s-s combinations the contribution to either $J^1_{\mathrm{F}^-}$ or $J^1_{\mathrm{Li}^+}$ is

$$-4\pi\int_0^\infty d\rho\,\rho[S^{0,h}_{\mathrm{Li},\,\mathrm{F}\,1s}\,\chi_{\mathrm{F}\,1s}(p)+S^{0,h}_{\mathrm{Li},\,\mathrm{F}\,2s}\,\chi_{\mathrm{F}\,2s}(p)]\,\chi_{\mathrm{Li}}(p)$$
$$\times\sum_h^{\text{1st shell}} J_0(\rho R_{h,\parallel})\cos(p_z R_{h,\perp}) \tag{28}$$

with

$$p=(\rho^2+p_z^2)^{1/2}\quad . \tag{29}$$

For s-p combinations we have similarly

$$4\pi\int_0^\infty d\rho\,\rho\chi_{\mathrm{Li}}(p)\,\chi_{2p}(p)$$
$$\times\sum_h^{\text{1st shell}}[S^{0,h}_{\mathrm{Li},\,\mathrm{F}\,2p_x}\,\rho J_1(\rho R_{h,\parallel})\cos(p_z R_{h,\perp})$$
$$+S^{0,h}_{\mathrm{Li},\,\mathrm{F}\,2p_z}\,p_z J_0(\rho R_{h,\parallel})\sin(\rho_z R_{h,\perp})]\ . \tag{30}$$

In Eq. (30) the overlap integral is to be evaluated with the Li⁺ orbital on the central site. The second shell and p-p combinations give

$$-4\pi\int_0^\infty d\rho\,\rho\chi^2_{\mathrm{F}\,2p}(p)\sum_h^{\text{2nd shell}}[S_{\mathrm{F}\,2p_x,\,\mathrm{F}\,2p_x}$$
$$\times\rho^2 J_1(\rho R_{h,\parallel})\cos(p_z R_{h,\perp})+S_{\mathrm{F}\,2p_y,\,\mathrm{F}\,2p_y}\,\rho J_1(\rho R_{h,\parallel})$$
$$\times\cos(p_z R_{h,\perp})/R_{h,\parallel}+S_{\mathrm{F}\,2p_z,\,\mathrm{F}\,2p_z}\,p_z^2 J_0(\rho R_{h,\parallel})\cos(p_z R_{h,\perp})$$
$$-2S_{\mathrm{F}\,2p_x,\,\mathrm{F}\,2p_z}\,\rho p_z J_1(\rho R_{h,\parallel})\sin(p_z R_{h,\perp})]\ . \tag{31}$$

Expressions (28)–(31) are to be evaluated in coordinate system (II), i.e., a different system for each pair of ions. The remaining contributions to J^1 are all similar to the expressions above. Furthermore, all the contributions are even in p_z, i.e., $J^1(p_z)$ is an even function.

Finally, if the ion solutions are assumed to be linear combinations of Slater-type orbitals also the integration over ρ can be performed analytically. This is described in Appendix A.

D. Evaluation of $J^2(p_z)$

With the $2p$ orbitals oriented as in coordinate system (II) the integration over the angle ϕ is trivial. We obtain for the F⁻ ion

$$J^2_{\mathrm{F}^-}(p_z)=4\pi\int_0^\infty d\rho\,\rho[(\tilde{S}^2)^{0,0}_{\mathrm{F}\,1s,\,\mathrm{F}\,1s}\,\chi^2_{\mathrm{F}\,1s}(p)+(\tilde{S}^2)^{0,0}_{\mathrm{F}\,2s,\,\mathrm{F}\,2s}\,\chi^2_{\mathrm{F}\,2s}(p)+2(\tilde{S}^2)^{0,0}_{\mathrm{F}\,1s,\,\mathrm{F}\,2s}\chi_{\mathrm{F}\,1s}(p)\chi_{\mathrm{F}\,2s}(p)]$$
$$+2\pi\int_0^\infty d\rho\,\rho\,\chi^2_{2p}(p)[\rho^2(\tilde{S}^2)^{0,0}_{\mathrm{F}\,2p_x,\,\mathrm{F}\,2p_x}+\rho^2(\tilde{S}^2)^{0,0}_{\mathrm{F}\,2p_y,\,\mathrm{F}\,2p_y}+2p_z^2(\tilde{S}^2)^{0,0}_{\mathrm{F}\,2p_z,\,\mathrm{F}\,2p_z}]\ , \tag{32}$$

and similarly for the Li⁺ ion. Equation (32) can be simplified considerably, however. As discussed in Appendix B the required elements of $\tilde{S}^2$ are independent of the direction of the scattering vector. Furthermore we have

$$(\tilde{S}^2)^{0,0}_{\mathrm{F}\,2p_x,\,\mathrm{F}\,2p_x}=(\tilde{S}^2)^{0,0}_{\mathrm{F}\,2p_y,\,\mathrm{F}\,2p_y}$$
$$=(\tilde{S}^2)^{0,0}_{\mathrm{F}\,2p_z,\,\mathrm{F}\,2p_z}=(\tilde{S}^2)^{0,0}_{\mathrm{F}\,2p,\,\mathrm{F}\,2p}\quad . \tag{33}$$

Making the substitution in Eq. (29) we hence obtain

$$J^2_{\mathrm{F}^-}(p_z)=4\pi\int_{|p_z|}^\infty dp\,p[(\tilde{S}^2)^{0,0}_{\mathrm{F}\,1s,\,\mathrm{F}\,1s}\,\chi^2_{\mathrm{F}\,1s}(p)$$
$$+(\tilde{S}^2)^{0,0}_{\mathrm{F}\,2s,\,\mathrm{F}\,2s}\,\chi^2_{\mathrm{F}\,2s}(p)+2(\tilde{S}^2)^{0,0}_{\mathrm{F}\,1s,\,\mathrm{F}\,2s}\,\chi_{\mathrm{F}1s}(p)\chi_{\mathrm{F}\,2s}(p)]$$
$$+4\pi(\tilde{S}^2)^{0,0}_{\mathrm{F}\,2p,\,\mathrm{F}\,2p}\int_{|p_z|}^\infty dp\,p^3\,\chi^2_{2p}(p)\ , \tag{34}$$

$$J^2_{\mathrm{Li}^+}(p_z)=4\pi(\tilde{S}^2)^{0,0}_{\mathrm{Li},\,\mathrm{Li}}\int_{|p_z|}^\infty dp\,p\,\chi^2_{\mathrm{Li}}(p)\quad , \tag{35}$$

and

$$J^2(p_z)=J^2_{\mathrm{F}^-}(p_z)+J^2_{\mathrm{Li}^+}(p_z)\ . \tag{36}$$

The expression for $J^0(p_z)$ is obtained from Eqs. (34) and (35) if the matrix S^2 is replaced by the unit matrix.

It is clear from Eqs. (34) and (35) that $J^2(p_z)$ does not depend on the scattering vector. All directional properties of the Compton profile are thus contained in the linear term $J^1(p_z)$.

E. Normalization

The total Compton profile normalizes to the number of electrons N per Li⁺-F⁻ pair, i.e.,

$$\int_{-\infty}^\infty dp_z\,J(p_z)=N\ . \tag{37}$$

Since $J^0(p_z)$ is already normalized in accordance with Eq. (37) we obtain

$$\int_{-\infty}^\infty dp_z\,J^1(p_z)=-\int_{-\infty}^\infty dp_z\,J^2(p_z) \tag{38}$$

or

$$\int_0^\infty dp_z\,J^1(p_z)=-(\tilde{S}^2)^{0,0}_{\mathrm{Li},\,\mathrm{Li}}-(\tilde{S}^2)^{0,0}_{\mathrm{F}\,1s,\,\mathrm{F}\,1s}$$
$$-(\tilde{S}^2)^{0,0}_{\mathrm{F}\,2s,\,\mathrm{F}\,2s}-3(\tilde{S}^2)^{0,0}_{\mathrm{F}\,2p,\,\mathrm{F}\,2p}\quad . \tag{39}$$

The cross term in Eq. (34) disappears because of orthogonality.

Equation (39) constitutes a useful test for the calculation of $J^1(p_z)$. A similar test for the accuracy of the numerical work follows from expressions (28)–(31). From expression (28) we have, for example,

$$4\pi \int_0^\infty dp_z \int_0^\infty d\rho\, \rho\, \chi_{\mathrm{Li}}(p)\, \chi_{\mathrm{F\,1}s}(p)\, J_0(\rho R_{\parallel}) \times \cos(p_z R_{h,\perp}) = S_{\mathrm{Li,\,F\,1}s} \; . \qquad (40)$$

Other overlap integrals follow similarly.

V. THEORETICAL RESULTS

The Compton profile of LiF with the scattering vector along the ⟨100⟩, ⟨110⟩, and ⟨111⟩ axes have been calculated as described in Sec. IV. Three different sets of orbitals for the Li^+ and F^- ions have been used, namely, Clementi's free ion orbitals,[21] Kunz's[20] free ion orbitals and Kunz's orbitally relaxed crystal orbitals. The local orbital scheme does not automatically yield orthogonal solutions. The crystal orbitals were therefore orthogonalized, although in the case of LiF this led to only small corrections. In the calculations we have included all contributions up to the fourth shell. By then the contributions were sufficiently small to terminate the summations over the lattice in order to save computer time. The normalization conditions in Eqs. (37)–(40) were checked for the three scattering vectors mentioned as well as for some very odd ones. The calculated anisotropies are shown in Figs. 7–9 together with the results of Euwema *et al.*[10] The various contributions to the total profile are given in Table III for the case of Kunz's self-consistent crystal orbitals.

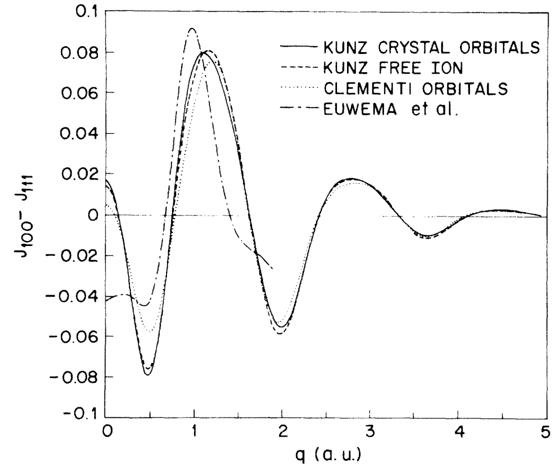

FIG. 7. Unsmeared difference between ⟨100⟩ and ⟨111⟩ Compton profiles as obtained from different wave functions. The dotted curve refers to Clementi's free ion solutions, the dashed curve to Kunz's free ion solutions, and the full drawn curve to Kunz's orbitally relaxed crystal solucitons Results of Euwema *et al.* are denoted by the dash-dot curve.

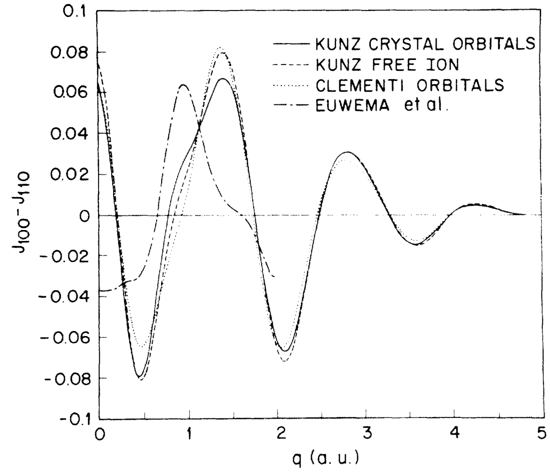

FIG. 8. Unsmeared difference between ⟨100⟩ and ⟨110⟩ Compton profiles obtained from different wave functions. Notations are the same as in Fig. 7.

In Figs. 7–9 there is an overall qualitative agreement between the anisotropies as calculated from our three different choices of ionic orbitals. The numerical differences that result from Clementi's and Kunz's free ion solutions merely reflect the use of slightly different basis functions in Eq. (A2). Ideally the curves corresponding to these two wave functions should of course coincide. The differences resulting from Kunz's two sets of orbitals are, on the other hand, real. Their smallness indicates, however, that relaxation owing to the crystal environment is not an important effect in LiF. These differences become even less significant when the theoretical profiles are convoluted

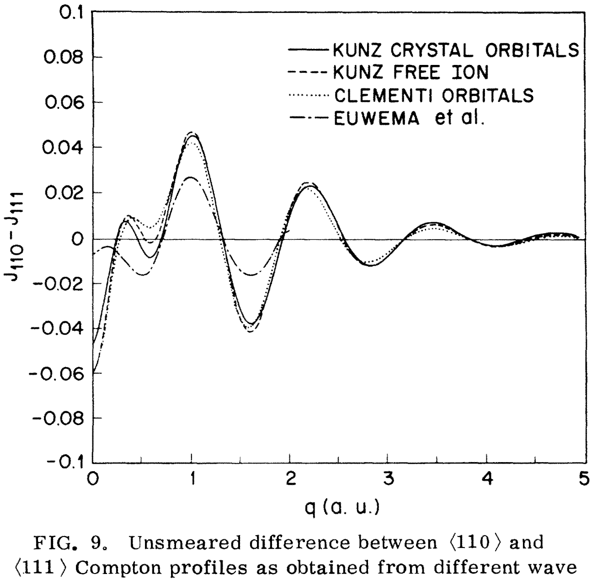

FIG. 9. Unsmeared difference between ⟨110⟩ and ⟨111⟩ Compton profiles as obtained from different wave functions. Notations are the same as in Fig. 7.

TABLE III. Different contributions to the directional Compton profile for LiF as calculated from Kunz's orbitals (unsmeared results).

q (a.u.)	J^0	J^1_{100}	J^1_{110}	J^1_{111}	J^2	q (a.u.)	J^0	J^1_{100}	J^1_{110}	J^1_{111}	J^2
0.0	4.0790	−0.3254	−0.3899	−0.3428	0.1185	2.0	0.7735	−0.0572	+0.0035	−0.0015	0.0210
0.1	4.0618	−0.3300	−0.3771	−0.3405	0.1182	2.1	0.7021	−0.0519	0.0157	−0.0010	0.0187
0.2	4.0110	−0.3420	−0.3452	−0.3319	0.1173	2.2	0.6390	−0.0386	0.0222	−0.0004	0.0166
0.3	3.9241	−0.3512	−0.3054	−0.3099	0.1155	2.3	0.5831	−0.0216	0.0223	+0.0003	0.0148
0.4	3.7887	−0.3368	−0.2608	−0.2669	0.1123	2.4	0.5335	−0.0053	0.0172	0.0008	0.0132
0.5	3.5955	−0.2811	−0.0247	−0.2018	0.1072	2.5	0.4895	−0.0072	0.0088	0.0010	0.0117
0.6	3.3518	−0.1870	−0.1331	−0.1244	0.1003	2.6	0.4504	0.0148	0.0001	0.0010	0.0105
0.7	3.0773	−0.0775	−0.0537	−0.0512	0.0922	2.7	0.4155	0.0181	−0.0075	0.0007	0.0093
0.8	2.7937	+0.0195	+0.0178	+0.0039	0.0837	2.8	0.3844	0.0185	−0.0118	0.0002	0.0083
0.9	2.5173	0.0857	0.0676	0.0353	0.0753	2.9	0.3566	0.0173	−0.0126	−0.0002	0.0075
1.0	2.2583	0.1174	0.0894	0.0457	0.0674	3.0	0.3316	0.0149	−0.0103	−0.0004	0.0067
1.1	2.0214	0.1215	0.0849	0.0419	0.0601	3.1	0.3092	0.0117	−0.0061	−0.0005	0.0060
1.2	1.8080	0.1088	0.0617	0.0316	0.0535	3.2	0.2890	0.0076	−0.0012	−0.0004	0.0054
1.3	1.6175	0.0881	0.0296	0.0203	0.0476	3.3	0.2707	0.0027	+0.0030	−0.0002	0.0048
1.4	1.4482	0.0644	−0.0017	0.0110	0.0424	3.4	0.2541	−0.0023	+0.0058	+0.0000	0.0043
1.5	1.2984	0.0392	−0.0253	0.0047	0.0377	3.5	0.2390	−0.0065	0.0067	0.0002	0.0039
1.6	1.1659	0.0127	−0.0372	0.0010	0.0335	3.6	0.2253	−0.0091	0.0058	0.0002	0.0035
1.7	1.0489	−0.0136	−0.0370	−0.0009	0.0298	3.7	0.2127	−0.0097	0.0037	0.0002	0.0032
1.8	0.9455	−0.0365	−0.0272	−0.0017	0.0265	3.8	0.2012	−0.0085	0.0011	0.0001	0.0029
1.9	0.8542	−0.0519	−0.0122	−0.0018	0.0236	3.9	0.1905	−0.0061	−0.0013	−0.0001	0.0026
						4.0	0.1807	−0.0033	−0.0030	−0.0001	0.0023

with the experimental resolution function as shown in Fig. 10. For this reason we have only considered Kunz's crystal orbitals in the final comparison with experiments in Figs. 3–5. It is clear, however, that the results of Euwema *et al.*[10] differ distinctly from ours before as well as after convolution.

Table IV lists unsmeared and smeared theoretical results for the ⟨100⟩ direction for comparison with the experimental results in Table I. The two sets of data are also displayed in Fig. 11.

VI. DISCUSSION AND COMPARISON

Previous Compton measurements of LiF have been reported by Weiss[3] and Paakkari *et al.*[9] using Mo $K\alpha$ x rays and 59.54-keV γ rays from an ^{241}Am source, respectively. Weiss measured a value of $J(0) = 3.78 \pm 0.11$ which is in reasonable agreement with either our measured value for the 0.178-mm thick sample or the value we obtain when extrapolating to zero thickness.[22] Paakkari *et al.* report a value of $J(0) = 3.85 \pm 0.05$ for polycrystalline LiF in good agreement with present measurements.

There have been several attempts to calculate the Compton profile of polycrystalline LiF. Weiss[3] showed that the simple summation of the profiles for the free Li^+ and F^- ions is not adequate since it predicts too narrow a profile and a $J(0) = 4.10$. The same discrepancy is illustrated in Fig. 11 for the ⟨100⟩ profile. Berggren,[7] Aikala *et al.*[8] and Paakkari *et al.*[9] have included overlap effects between the free ions in the same way as discussed in Sec. IV A and find that these effects do reduce the value of $J(0)$. Aikala *et al.*[8] and Paakkari *et al.*[9] calculated a value of $J(0) = 3.86$ and 3.83, respectively, for the average profile which is in good agreement with our measured value.[22] For this reason it has been natural to extend this type of calculations to include also effects of anisotropy (Sec. IV).

A recent calculation of LiF is by Euwema *et al.*[10] who used a self-consistent Hartree-Fock scheme to calculate the Compton profile for various crystallographic directions. Besides that the Hartree-Fock energy bands, cohesive energy, equilibrium lattice parameter, bulk modulus, and x-ray structure factors were also considered. Their absolute profile for J_{100} convoluted with our resolution function agrees with our zero thickness estimate such

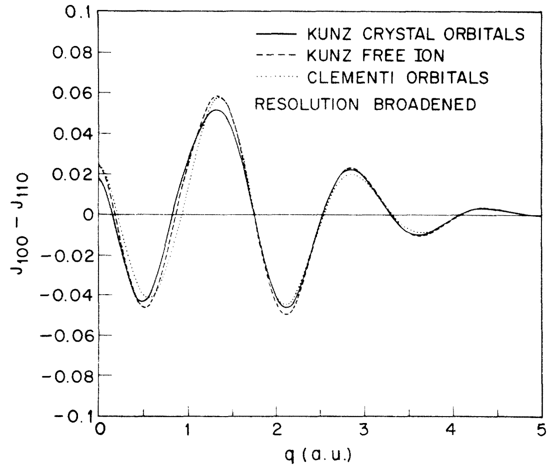

FIG. 10. Smeared difference between ⟨100⟩ and ⟨110⟩ Compton profiles as obtained from different wave functions. Notations are the same as in Fig. 7.

TABLE IV. Theoretical Compton profiles for LiF—⟨100⟩. Present calculation refers to Kunz's self-consistent crystal orbitals.

q (a.u.)	Present calculation	Euwema *et al.*[a]	Present calculation[b]	Euwema *et al.*[c]
0.0	3.872	3.839	3.795	3.777
0.1	3.850	3.825	3.777	3.766
0.2	3.786	3.779	3.723	3.715
0.3	3.688	3.700	3.637	3.638
0.4	3.564	3.586	3.524	3.535
0.5	3.422	3.446	3.388	3.406
0.6	3.265	3.290	3.231	3.255
0.7	3.092	3.122	3.055	3.084
0.8	2.897	2.938	2.862	2.894
0.9	2.678	2.728	2.653	2.685
1.0	2.443	2.489	2.434	2.461
1.1	2.203		2.213	2.228
1.2	1.970	1.968	1.994	1.996
1.3	1.753		1.784	1.774
1.4	1.555	1.515	1.588	1.570
1.5	1.375		1.408	1.388
1.6	1.212	1.181	1.245	1.228
1.7	1.065		1.099	1.090
1.8	0.936	0.940	0.972	0.969
1.9	0.826		0.863	0.861
2.0	0.737	0.757	0.772	0.763
2.2	0.617		0.638	
2.5	0.508		0.511	
3.0	0.353		0.356	
3.5	0.236		0.242	
4.0	0.180		0.181	

[a] From Ref. 10.

[b] Convoluted with experimental resolution function.

[c] From Ref. 10: convoluted with experimental resolution function.

that $\Delta J/J(0)=0.8\%$ and $\Delta J/J(q)\leq 4.5\%$ for $0\leq q\leq 2$ a.u.

The dashed lines in Figs. 3–5 are the anisotropies calculated by Euwema *et al.* after being convolved with our resolution function. As can be seen the agreement with the experimental results is not particularly good except for J_{110}-J_{111}. However this difference is for the two "nonbonding" directions. In diamond,[2] silicon, and germanium[1] it has previously been shown that the "nonbonding" directions are insensitive to the potential used in the calculation and the difference between profiles for these directions fit the data quite well. It is the difference between the profiles for the bonding and nonbonding directions which is the best test of a calculation.

By comparing the results in Table I for the ⟨100⟩ direction and the anisotropy results in Table II one can conclude that the experiment and theory of Euwema *et al.* agree for the ⟨100⟩ in the region around $q=0$ but the theory predicts too much momentum around $q=1$ and too little at high q. For the ⟨110⟩ and ⟨111⟩ directions the opposite is true, the theory and experiment agree around $q=1$ but theory predicts too much around $q=0$ and too little at high q. As a general observation one could characterize the theory as not having enough high momentum components in its description of the bond and that these high momentum components tend to reduce the low momentum anisotropy and introduce the presence of high momentum anisotropies not even predicted by the theory. In other words the amount of the "bond charge" is probably the same in both theory and experiment but appears to be less localized in the Euwema calculations.

A comparison of Tables I and IV shows that there is a good agreement between the present theory and experiment as illustrated in Fig. 11. We obtain $\Delta J(0)=0.3\%$ and $\Delta J/J(q)\leq 3.3\%$ for $0\leq q\leq 2$. As stressed above, however, the anisotropies themselves provide a much severer test of the quality of the crystal wave function. From Figs. 3–5 it is evident that the present tight-binding model removes the deficiencies associated with the Hartree-Fock solution of Euwema *et al.*,[10] and that there is now a satisfactory overall agreement between calculated and measured anisotropies.

One may ask why the theory of Euwema *et al.*, which is quite successful in many other respects, fails to predict the correct anisotropy in Compton scattering. A possible reason may be their choice of a Gaussian basis. The difficulties of properly describing the tails of wave functions with such a

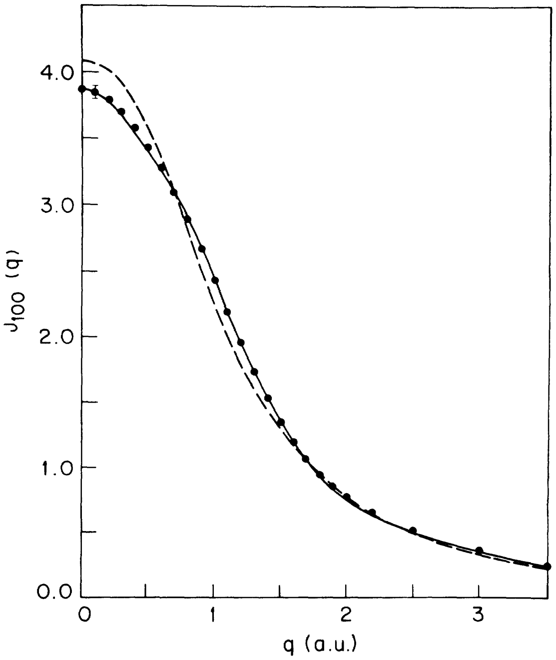

FIG. 11. Total ⟨100⟩ Compton profile for LiF. Solid curve refers to Kunz's self-consistent crystal solutions, and the dashed curve to a simple superposition of free ion solutions. Dots are experimental values from Table I, as corrected for instrumental resolution and multiple scattering. The bar at $q=0.1$ a.u. denotes the estimated experimental error.

basis are well known. A further difficulty is their use of Gaussian lobes rather than proper p functions. Besides that Gaussian contractions appropriate to free atoms were used, whereas contractions appropriate to Li^+ and F^- should have been a better choice as remarked by Euwema *et al.* This fact resulted in certain difficulties in predicting the correct binding energy. Only when a separate Hartree-Fock calculation using the same contracted basis together with some additional longer-range Gaussians was performed for the free Li^+ and F^- ions was a correct binding energy obtained . The lack of these longer-range Gaussians in the original basis and perhaps the use of Gaussians in general should be reflected in an inadequate description of the low momentum region.

Finally we compare our calculated profiles with the experimental values of Paakkari *et al.*[9] for polycrystalline LiF. We may compute an approximate spherical average as

$$J = \frac{1}{26}(6J_{100} + 12J_{110} + 8J_{111}) \quad . \tag{41}$$

Table V lists this weighted average as computed from Kunz's crystal orbitals and the experimental values of Paakkari *et al.* One finds $\Delta J/J(0) = 0.3\%$ and $\Delta J/J(q) \leq 1.5\%$ for $0 \leq q \leq 2$. As mentioned Paakkari *et al.* have also performed a theoretical calculation of the isotropic Compton profile. Their calculation consists basically in taking a spherical average of the momentum density in Eq. (15) which is then integrated in accordance with Eq. (22). In order to allow for orbital relaxation the outermost orbitals were supplemented by a scaling factor, which was then determined from minimization of the total energy. Their theoretical results should therefore compare well with Table V which refers to relaxed orbitals as well. We obtain $\Delta J/J(0) = 0.2\%$ and $\Delta J/J(q) \leq 0.5\%$ for $0 \leq q \leq 2$. Although we have stressed earlier that the most meaningful test of wave functions consists in comparing anisotropies we find it quite satisfying that our calculations agree so well with two independent sets of experimental data recorded with 59.54- and 159-keV γ rays, respectively, and with a similar, but isotropic calculation.

Another interesting result of this work is that we can now understand the apparent paradox between the charge-density anisotropy, as measured by elastic x-ray scattering, and the momentum density anisotropy, as measured by Compton scattering.[11] The most recent conclusion drawn from an analysis of elastic x-ray scattering measurements[23–26] is that the charge density, to within the experimental accuracy, is isotropic, i.e., the charge is spherically symmetrical about each ion.[26] It is clear from our Compton measurements that the momentum density is not isotropic. Since Compton scattering unlike elastic x-ray scattering is related to both the off-diagonal and diagonal elements of the single-particle density matrix $\rho(\vec{r}, \vec{r}\,')$, one would expect it to yield more complete information about these anisotropies. Both our experimental and theoretical results indicate that this is indeed the case.

The formal definition for the Compton profile for a one-electron wave function $\chi(\vec{r})$ and the momentum transfer $\vec{k}$ is given by Eqs. 4, 5, and 14 and the form factor by

$$F(\vec{k}) = \int e^{-i\vec{k}\cdot\vec{r}}\,|\chi(r)|^2 d\vec{r} \quad . \tag{42}$$

For the case of periodic systems such as LiF one has, of course, that $\vec{k}$ in $F(\vec{k})$ is limited to reciprocal-lattice vectors, whereas there is no such restriction for the Compton profile.

The explanation lies in the dependency of the elastic scattering factors on only the diagonal elements of the single-particle density matrix $\rho(\vec{r}, \vec{r}\,')$. This results in a "smearing out" of anisotropies, as compared with Compton scattering. For any form of anisotropic charge density the anisotropy in the Compton profile is orders of magnitude larger than that for the form factor for smaller values of q, and the smaller the magnitude of the anisotropy, the larger the q values at which the most significant part of the form-factor anisotropy occurs. In the case where the anisotropy results from overlapping charges, the anisotropy of the Compton profile goes linearly with the overlap, whereas the form-factor anisotropy goes effectively worse than the square of the overlap.[27,28] Furthermore there is a coherent constructive enhancement in certain directions of momentum space which increases the Compton anisotropy, and in most cases no such enhancement occurs in elastic scattering. These effects

TABLE V. Comparison between the weighted average $\langle J \rangle$ of theoretical directional Compton profiles and the experimental data of Paakkari *et al.* for polycrystalline LiF. Theoretical results refer to Kunz's self-consistent crystal orbitals.

q (a.u.)	$\langle J \rangle$	$J^{\text{expt a}}$	q (a.u.)	$\langle J \rangle$	$J^{\text{expt a}}$
0.0	3.837	3.85 ± 0.05	1.4	1.508	1.52
0.1	3.825	3.82	1.5	1.334	1.33
0.2	3.788	3.78	1.6	1.186	1.18
0.3	3.722	3.70	1.8	0.950	0.94
0.4	3.620	3.61 ± 0.04	2.0	0.782	0.77 ± 0.02
0.5	3.481	3.48	2.5	0.507	0.51
0.6	3.309	3.32	3.0	0.337	0.34 ± 0.01
0.7	3.111	3.12	3.5	0.245	0.24
0.8	2.891	2.90	4.0	0.181	0.19
0.9	2.654	2.67	5.0	0.114	0.11
1.0	2.408	2.43	6.0	0.076	0.08
1.2	1.925	1.95 ± 0.03			

[a] From Ref. 9 (data corrected for instrumental resolution).

are simply illustrated in the case of an ionic crystal with small overlap, where we may expand the wave functions in the overlap. Then the leading anisotropic part of the form factor owing to an orbital of type α at site $\vec{R}_g$ overlapping an orbital of type β at site $\vec{R}_h$, at wave vector $\vec{k}$ is given by

$$2S^{gh}_{\alpha\beta}\int \chi^*_\alpha(\vec{r}-\vec{R}_g)\chi_\beta(\vec{r}-\vec{R}_h)\, e^{i\vec{k}\cdot\vec{r}}\, d\vec{r} \quad , \tag{43}$$

where the overlap is given by Eq. 13.

$$S^{gh}_{\alpha\beta} = \int \chi^*_\alpha(\vec{r}-\vec{R}_g)\, \chi_\beta(\vec{r}-\vec{R}_h)\, d\vec{r} \quad . \tag{44}$$

The anisotropic part clearly goes as overlap times the Fourier transform of overlap which is thus less than the overlap squared. The equivalent term for the Compton profile is given by

$$2S^{gh}_{\alpha\beta}\int \chi^*_\alpha(\vec{p})\, \chi_\beta(\vec{p})\, e^{i\vec{p}\cdot(\vec{R}_g-\vec{R}_h)}\, dp_x\, dp_y \quad . \tag{45}$$

The Fourier transforms are given by Eq. (16) and clearly are not site dependent and thus do not overlap in p space. The constructive enhancement mentioned above comes from the expression $e^{i\vec{p}\cdot(\vec{R}_g-\vec{R}_h)}$ in the Compton profile which has become known as the diffraction effect.[29] Calculations of LiF show that $\Delta F/F(0)$ is orders of magnitude smaller than $\Delta J/J(0)$ over the range of q or k for which either $J(q)$ or $F(k)$ is larger than a few percent of its maximum. For example we find that the anisotropy of the form factors[6] $[F(511) - F(333)]/F(0) \approx 1\times 10^{-5}$ and $[F(711) - F(511)]/F(0) < 10^{-5}$ which approximate the anisotropies [100] − [111] and [100] − [110], respectively. From Figs. 3–5 one sees that $\Delta J/J(0)$ is of the order 10^{-2} to 10^{-3}. Typical values for nearest-neighbor overlap $S_{\alpha\beta}$ in Lif are 10^{-2} and thus the fact that form-factor anisotropies depend upon $S^2_{\alpha\beta}$ while Compton profile anisotropies vary only as $S_{\alpha\beta}$ explains the 10^2 larger anisotropy in the Compton profile. We conclude that to measure the anisotropy in the charge distributions in LiF by elastic x-ray scattering, the experiments would have to be several orders of magnitude more accurate.[11]

Yet there are factors which make it very difficult to obtain in elastic scattering an accuracy even as good as that obtainable by Compton scattering. Among these are large corrections for systematic effects such as extinction. In addition one can only measure the form factor at discrete values of k. Thus both the physics and the nature of the experiments dictate the use of the Compton-scattering technique to measure anisotropies in electron distributions.

VII. SUMMARY

We have measured the Compton profiles of LiF in the ⟨100⟩, ⟨110⟩, and ⟨111⟩ directions using 159-keV γ rays and find that the anisotropy of the momentum distribution of this ionic crystal to be as large as that found in some covalent crystals. On the basis of a tight-binding model we have performed theoretical calculations of the anisotropies using three different sets of ion wave functions. The results of these calculations agree well among each other as well as with the measured anisotropies. They also indicate that the distortion of the ions owing to the crystal environment is quite negligable in LiF.

Our results are found to compare well with the isotropic Compton profile obtained recently by means of 59.54-keV γ rays and with isotropic calculations based on a tight-binding model similar to ours.[2] Hartree-Fock calculations of the directional Compton profile by Euwema *et al.*[10] are shown not to agree as well with measured values, particularly in the region of small momentum transfer. A possible reason for this is given.

We also show that Compton scattering is more sensitive to anisotropy in the momentum distribution than x-ray form factors are to the anisotropy in the charge density, at least for those materials with small overlap of their wave functions. This resolves the apparent paradox between Compton- and elastic x-ray scattering results.

ACKNOWLEDGMENTS

One of the authors (K.-F. B) was partly supported by Stanford Synchrotron Radiation Project through NSF Grant GP-38325 and the Swedish Natural Science Research Council. He would like to thank Professor S. Doniach for hospitality during a stay at Stanford University.

APPENDIX A

The one-electron functions (dropping the index referring to the lattice site) are both in Clementi's[21] and Kunz's[20] calculations assumed to be of the form

$$\chi_{nl}(\vec{r}) = R_{nl}(r)\, Y^m_l(\theta, \phi) \quad . \tag{A1}$$

In Eq. (A1) $Y^m_l(\theta, \phi)$ is a spherical harmonic function which we here chose to be real. The radial part $R_{nl}(r)$ is then expanded in terms of Slater-type orbitals,

$$\begin{gathered} rR_{nl}(r) = \sum_j C_{jnl}\, P_{jl}(r) \quad , \\ P_{jl}(r) = N_{lj}\, r^{l+1+n_{lj}}\, e^{-\alpha_{lj} r} \quad , \\ N_{lj} = [(2\alpha_{lj})^{2l+2n_{lj}+3}/(2l+2n_{lj}+2)!\,]^{1/2} \quad . \end{gathered} \tag{A2}$$

In the case of LiF the expansion includes Slater-type orbitals of $1s$, $2s$, and $2p$ type only. The momentum transform [Eq. (16)] of $\chi_{nl}(\vec{r})$ can hence be written

$$\langle \vec{p}\,|nl\rangle = \sum_j C_{jnl}\, \langle \vec{p}\,|jl\rangle \quad , \tag{A3}$$

where $\langle \vec{p}\,|jl\rangle$ refers to the basis functions transformed to momentum space. For Slater-type orbitals of $1s$ and $2s$ type we have in particular

$$\langle\vec{\mathrm{p}}\,|\,1s\rangle=(4\alpha^{5/2}/\pi\sqrt{2})\,[1/(\alpha^2+p^2)^2] \tag{A4}$$

$$\langle\vec{\mathrm{p}}\,|\,2s\rangle=-\frac{4}{\pi\sqrt{6}}\frac{\alpha^{5/2}}{(\alpha^2+p^2)^2}\left(1-\frac{4\alpha^2}{\alpha^2+p^2}\right)\ , \tag{A5}$$

where the indices (jl) have been dropped. For $2p$ type functions the transform is

$$\langle\vec{\mathrm{p}}\,|\,2p\rangle=i(16\alpha^{7/2}/\pi\sqrt{2})\,[\vec{\mathrm{p}}/(\alpha^2+p^2)^3]\ . \tag{A6}$$

Given these analytical forms the computation of the anisotropic Compton profile is immensely facilitated since all the contributions can be evaluated in a closed form. Integrals like those appearing in the expression for $J_1(p_z)$ [Eqs. (28)–(31)] now reduce to the basic form

$$I=\int_0^\infty d\rho\,\rho^{l+1}\frac{J_l(\rho R)}{(a^2+\rho^2)^{n+1}(b^2+\rho^2)^{m+1}}\ , \tag{A7}$$

where $a^2=\alpha^2_{lj}+p_z^2$ and $b^2=\alpha^2_{l'j'}+p_z^2$. For $a=b$ Eq. (A7) is a Hankel-Nicholson-type integral[30]

$$\int_0^\infty d\rho\,\frac{\rho^{l+1}J_l(\rho R)}{(\rho^2+a^2)^{n+1}}=\left(\frac{R}{2a}\right)^n\frac{a^l}{n!}K_{l-n}(aR)\ , \tag{A8}$$

where $K_n(x)$ are modified Bessel functions of the second kind. For $a\neq b$ it is convenient to write

$$\frac{1}{(\rho^2+a^2)(\rho^2+b^2)}=\frac{1}{b^2-a^2}\left(\frac{1}{\rho^2+a^2}\ \frac{1}{\rho^2+b^2}\right)\ . \tag{A9}$$

Repeated differentiation with respect to a^2 and b^2 then gives

$$\begin{aligned}\int_0^\infty d\rho\,&\frac{\rho^{l+1}J_l(\rho R)}{(\rho^2+a^2)^{n+1}(\rho^2+b^2)^{m+1}}\\&=\frac{1}{m!}\sum_{k=0}^{n}(-1)^k\frac{(m+k)!}{k!\,(n-k)!}\left(\frac{R}{2a}\right)^{n-k}\frac{a^l}{(b^2-a^2)^{m+k+1}}\\&\quad\times K_{n-k-l}(aR)+\frac{1}{n!}\sum_{k=0}^{m}(-1)^k\frac{(n+k)!}{k!\,(m-k)!}\left(\frac{R}{2b}\right)^{m-k}\\&\quad\times\frac{b^l}{(a^2-b^2)^{n+k+1}}K_{m-k-l}(bR)\ .\end{aligned} \tag{A10}$$

Differentiation of this expression with respect to R gives the remaining integrals in the expression for $J^1(p_z)$. The integrals appearing in the evaluation of $J^0(p_z)$ and $J^2(p_z)$ are all elementary.

APPENDIX B

We want to show that the sum in expression (26) is independent of any particular coordinate system. Assume that the two coordinate systems I and II in Fig. 6 are related as

$$\tilde{r}'=\tilde{r}\tilde{U}\ , \tag{B1}$$

where U is a unitary transformation matrix and $\tilde{r}^{(\prime)}=(x^{(\prime)},\,y^{(\prime)},\,z^{(\prime)})$. Since the $2p$ orbitals transform in the same way as $\tilde{r}$ we may write

$$\langle\vec{\mathrm{p}}\,|\,\tilde{\alpha}\rangle=\langle\vec{\mathrm{p}}\,|\,\tilde{\alpha}\rangle\,\tilde{V}\ , \tag{B2}$$

where $\langle\vec{\mathrm{p}}\,|\,\tilde{\alpha}\rangle$ is a row vector consisting of the momentum transforms of the F^- orbitals, and

$$\tilde{V}=\begin{pmatrix}\tilde{1}&\tilde{0}\\\tilde{0}&\tilde{U}\end{pmatrix}\ . \tag{B3}$$

In the case of a F^--F^- pair the overlap integrals transform as

$$\langle\tilde{\alpha}'\,|\,\tilde{\beta}'\rangle=\tilde{V}^+\langle\tilde{\alpha}\,|\,\tilde{\beta}\rangle\,\tilde{V}\ , \tag{B4}$$

where we have used the notation

$$S^{0,h}=\langle\tilde{\alpha}\,|\,\tilde{\beta}\rangle\ . \tag{B5}$$

The invariance of expression (26) then follows from

$$\begin{aligned}\langle\vec{\mathrm{p}}\,|\,\tilde{\alpha}\rangle\langle\tilde{\alpha}'\,|\,\tilde{\beta}'\rangle\langle\tilde{\beta}'\,|\,\vec{\mathrm{p}}'\rangle&=\langle\vec{\mathrm{p}}\,|\,\tilde{\alpha}\rangle\,\tilde{V}\tilde{V}^+\langle\tilde{\alpha}\,|\,\tilde{\beta}\rangle\,\tilde{V}\tilde{V}^+\langle\tilde{\beta}\,|\,\vec{\mathrm{p}}\rangle\\&=\langle\vec{\mathrm{p}}\,|\,\tilde{\alpha}\rangle\langle\tilde{\alpha}\,|\,\tilde{\beta}\rangle\langle\tilde{\beta}\,|\,\vec{\mathrm{p}}\rangle\ ,\end{aligned} \tag{B6}$$

since $\tilde{V}\tilde{V}^+=\tilde{1}$. In the case of a Li^+-F^- pair the invariance follows in a similar way.

In a similar way one may show that the required elements of $\tilde{S}^2$ are independent of any particular coordinate system and thereby the orientation of the p orbitals. For p functions a summation over the lattice is, however, also required.

Note added in proof: Recently Euwema has followed up our suggestion of contracting his basis to the ionic rather than the atomic wave functions (Ref. 10). This change plus the use of a tight Li p basis function result in significant improvement in the calculated anisotropies. The binding energy remains close to that of the earlier calculation. This would seem to be another indication of the extreme sensitivity of the Compton anisotropies to the quality of the wave functions.

We are grateful to Dr. R. N. Euwema for correspondence and for sending us his unpublished results.

---

[1] W. A. Reed and P. Eisenberger, Phys. Rev. B 6, 4596 (1972).

[2] W. A. Reed, P. Eisenberger, K. C. Pandey, and L. C. Snyder, Phys. Rev. B 10, 1507 (1974).

[3] R. J. Weiss, Philos. Mag. 21, 1169 (1970).

[4] P.-O. Löwdin, *A Theoretical Investigation into Some Properties of Ionic Crystals* (Almqvist and Wiksell, Upsala, Sweden, 1948).

[5] P.-O. Löwdin, Philos. Mag. Suppl. 5, 1 (1956).

[6] O. Aikala and K. Mansikka, Phys. Kondens. Mater. 11, 243 (1970); *ibid.* 14, 105 (1972).

[7] K.-F. Berggren, Solid State Commun. 9, 861 (1971).

[8] O. Aikala, V. Jokela, and K. Mansikka, J. Phys. C 6, 1116 (1973).

[9] T. Paakkari, E.-L. Kohonen, O. Aikala, M. Mansikka, and S. Mikkola, Phys. Fenn. 9, 207 (1974).

[10] R. N. Euwema, G. G. Wepfer, G. T. Surratt, and D. L. Wilhite, Phys. Rev. B 9, 5249 (1974).

[11] W. A. Reed, P. Eisenberger, F. Martino, and K.-F. Berggren, Phys. Rev. Lett. 35, 114 (1975).

[12] P. M. Platzman and N. Tzoar, Phys. Rev. 139, 410 (1965).

[13] P. Eisenberger and P. M. Pltazman, Phys. Rev. 172, 415 (1970).

[14] P. Eisenberger and W. A. Reed, Phys. Rev. B 9, 3237 (1974).

[15] P. Eisenberger and W. A. Reed, Phys. Rev. A 5, 2085 (1972).

[16] P. Eisenberger and W. A. Reed, Phys. Rev. B 9, 3242 (1974).

[17] We have used a linear extrapolation to zero thickness for our two samples. Our results for zero thickness have been reconfirmed by a Monte-Carlo calculation of the effects of multiple scattering. (We are indebted to Dr. Joshua Felsteiner for having performed such calculations for us.)

[18] W. H. Adams, J. Chem. Phys. 34, 89 (1961); *ibid.* 37, 2009 (1962).

[19] T. L. Gilbert, in *Molecular Orbitals in Chemistry, Physics, and Biology*, edited by P. O. Löwdin and B. Pullman (Academic, New York, 1964).

[20] A. B. Kunz, Phys. Rev. B 2, 2224 (1970).

[21] E. Clementi, IBM J. Res. Dev. 9, 2 (1965).

[22] The profile for the two 1s electrons of F^+ must be added to the values reported in Refs. 3 and 8 before comparing them with our data.

[23] W. H. Zachariasen, Acta Crystallogr. A 24, 324 (1968).

[24] R. C. G. Killean, J. L. Lawrence, and V. C. Sharma, Acta Crystallogr. A 28, 405 (1972).

[25] C. J. Howard and R. G. Khadake, Acta. Crystallogr. A 30, 296 (1974).

[26] C. J. Howard and B. Dawson, International Crystallography Conference, Melbourne, Australia, 1974.

[27] W. H. Kleiner, J. Hanus, T. A. Kaplan, and H. E. Stanley, Bull. Am. Phys. Soc. 13, 483 (1968), and (unpublished).

[28] In the case of molecular-orbital-type one-electron wave functions, the Compton-profile anisotropy would be independent of overlap while the form factor would have a linear dependence on the Fourier transform of the overlap term. Thus the ratio of the anisotropic term in the form factor to that in the Compton profile would be the same as in our linear combination of atomic orbitals approach.

[29] C. A. Coulson, Proc. Camb. Philos. Soc. 37, 55 (1941).

[30] Y. L. Luke, in *Handbook of Mathematical Functions*, edited by M. Abramowitz and I. A. Stegun (National Bureau of Standards, Washington, 1964).